ISSN 0021-3640, JETP Letters, 2007, Vol. 85, No. 11, pp. 560–564. © Pleiades Publishing, Ltd., 2007.
Original Russian Text © V.D. Buchel'nikov, S.V. Taskaev, M.A. Zagrebin, P. Entel, 2007, published in Pis'ma v Zhurnal Éksperimental'noĭ i Teoreticheskoĭ Fiziki, 2007, Vol. 85, No. 11, pp. 689–693.

Phase Diagrams of Heusler Alloys with the Inversion of the Exchange Interaction

V. D. Buchel'nikov[a], S. V. Taskaev[a], M. A. Zagrebin[a], and P. Entel[b]

[a] *Chelyabinsk State University, Chelyabinsk, 454021 Russia*
e-mail: buche@csu.ru
[b] *Physics Department, University of Duisburg-Essen, Campus 47048 Duisburg, Germany*

Received April 5, 2007

The phase diagrams of magnetically ordered Heusler alloys with the inversion of the exchange interaction have been studied using the phenomenological Landau theory of phase transitions. It has been shown that the shape of the phase diagrams in these alloys depends on the magnitudes and signs of the phenomenological parameters in the Landau functional. At certain magnitudes and signs of the parameters of the Landau functional, the phase diagrams have thermodynamic paths that allow one to explain the experimentally observed sequences of the phase transitions in the Heusler alloys.

PACS numbers: 75.30.Ks, 75.50.-y, 75.80.+q

DOI: 10.1134/S0021364007110070

Studies on the properties of ferromagnetic Heusler alloys remain of considerable current interest because these alloys exhibit the magnetic shape memory effect in the ferromagnetic state and the giant magnetocaloric effect [1, 2]. The properties of the Ni–Mn–Ga Heusler alloys have been best studied to date. In these alloys, a structural (martensitic) phase transition from the high-temperature cubic (austenitic) phase to the low-temperature tetragonal (martensitic) phase and a magnetic phase transition from the paramagnetic phase to the ferromagnetic phase occur. In this case, the martensitic transformation can take place at a temperature that is either higher or lower than the Curie temperature. The structural and magnetic phase transitions coincide in some compositions [3, 4]. In this case, the above properties of the Ni–Mn–Ga alloys are most pronounced.

Recently, it was found that a structural phase transition accompanied by a transition from the ferromagnetic phase to the antiferromagnetic phase can occur in the Heusler alloys in addition to the magnetic phase transition from a paramagnetic to a ferromagnetic phase. It is likely that such a situation was observed in the $Ni_{45}Co_5Mn_{36.6}In_{13.4}$ Heusler alloy [5].

The phase diagrams of Ni–Mn–Ga alloys have been studied in sufficient detail [4, 6]. In a theoretical study of phase transitions in the Ni–Mn–Ga alloys, it was assumed that the sign of the exchange interaction remained unchanged in magnetically ordered phases; that is, all of the structural phases were ferromagnetic phases. It is well known that there are substances in which the magnetoelastic interaction can result in a change (inversion) of the sign of the exchange interaction [5, 7–9]. In these substances, a phase transition from a ferromagnetic phase to an antiferromagnetic phase occurs as the temperature is decreased. In the Heusler alloys, this transition is accompanied by a structural phase transition.

In this work, the phase diagrams of the Heusler alloys, in which the inversion of the exchange interaction can occur, are studied using the Landau theory of phase transitions.

Let us consider a two-sublattice antiferromagnetic structure with cubic symmetry. The free-energy density of the antiferromagnet can be written in the form

$$\begin{aligned} F &= \tilde{A}\mathbf{L}^2/2 + \tilde{B}\mathbf{L}^4/4 + \tilde{A}_1\mathbf{M}^2/2 + \tilde{D}(\mathbf{ML})^2/2 \\ &+ \tilde{D}'\mathbf{M}^2\mathbf{L}^2/2 + K(L_x^2L_y^2 + L_y^2L_z^2 + L_x^2L_z^2) \\ &+ K'(M_x^2M_y^2 + M_y^2M_z^2 + M_x^2M_z^2) - \mathbf{MH} + \tilde{B}_0e_1\mathbf{M}^2 \\ &+ G_0e_1\mathbf{M}^2 + \tilde{B}_1[e_2(L_x^2 - L_y^2)/2 + e_3(3L_z^2 - \mathbf{L}^2)/\sqrt{6}] \\ &+ G_1[e_2(M_x^2 - M_y^2)/2 + e_3(3M_z^2 - \mathbf{M}^2)/\sqrt{6}] \\ &+ \tilde{B}_2[e_4L_xL_y + e_5L_yL_z + e_6L_xL_z] \\ &+ G_2[e_4M_xM_y + e_5M_yM_z + e_6M_xM_z] - Ee_1 + E_0e_1^2/2 \\ &+ a(e_2^2 + e_3^2)/2 + c_{44}(e_4^2 + e_5^2 + e_6^2) + E_1e_1(e_2^2 + e_3^2) \\ &+ be_3(e_3^2 - 3e_2^2)/3 + c(e_2^2 + e_3^2)^2/4, \end{aligned} \quad (1)$$

where $\tilde{A}$, $\tilde{B}$, $\tilde{A}_1$, $\tilde{D}$, and $\tilde{D}'$; K and K'; and $\tilde{B}_i$ and G_i are exchange-interaction, anisotropy, and magnetostriction parameters, respectively; $\mathbf{M} = \mathbf{M}_1 + \mathbf{M}_2$ and $\mathbf{L} = \mathbf{M}_1 - \mathbf{M}_2$ are the ferromagnetism and antiferromag-

netism vectors, respectively; $\mathbf{M}_1$ and $\mathbf{M}_2$ are the sublattice magnetization vectors; $\mathbf{H}$ is the magnetic field intensity; e_i are the linear combinations of the strain tensor components, $e_1 = (e_{xx} + e_{yy} + e_{zz})/\sqrt{3}$, $e_2 = (e_{xx} - e_{yy})/\sqrt{2}$, $e_3 = (2e_{zz} - e_{yy} - e_{xx})/\sqrt{6}$, $e_4 = e_{xy}$, $e_5 = e_{yz}$, and $e_6 = e_{zx}$; E is a coefficient proportional to the thermal expansion coefficient; $E_0 = (c_{11} + 2c_{12})/\sqrt{3}$ is the bulk modulus; a, b, E_1, and c are the linear combinations of second-, third-, and fourth-order elastic moduli, respectively: $a = c_{11} - c_{12}$, $E_1 = (c_{111} - c_{123})/2\sqrt{3}$, $b = (c_{111} - 3c_{112} + 2c_{123})6\sqrt{6}$, and $c = (c_{1111} + 6c_{1112} - 3c_{1122} - 8c_{1123})/48$.

Let us consider the case where the sublattice magnetizations of the antiferromagnet are equal in magnitude and constant: $\mathbf{M}_1^2 = \mathbf{M}_2^2 = \mathbf{M}_0^2$. Under this condition, a magnetic subsystem can be described using a single variable φ, an angle between the antiferromagnetic sublattice magnetizations. In this work, in order to simplify the problem, we consider only the isotropic magnetic subsystem; that is, we ignore the magnetic anisotropy ($K = K' = 0$) and the anisotropic magnetostriction ($\tilde{B}_i$ and G_i, $i = 1, 2$) in Eq. (1). In this approximation, after the energy minimization of Eq. (1) with respect to the order parameters e_1, e_4, e_5, and e_6, which are not responsible for the phase transitions under consideration; the elimination of these parameters from energy (1); and the introduction of the angle φ, an expression for the free energy of the antiferromagnet can be significantly simplified and written in the form

$$F = A\cos\varphi + B\cos^2\varphi + D\cos\varphi(e_2^2 + e_3^2)/2 + a(e_2^2 + e_3^2)/2 + be_3(e_3^2 - 3e_2^2)/3 + c(e_2^2 + e_3^2)^2/4. \quad (2)$$

Here, the parameters A, B, and D, which have the dimensions of energy density, are expressed in terms of dimensionless constants in energy density (1) and the square of the saturation magnetization M_0. To simplify the calculations, we pass to dimensionless quantities. For this purpose, we redetermine parameters and variables in energy (2) as follows:

$$\bar{F} = c^3F/b^4, \quad \bar{e}_{2,3} = ce_{2,3}/|b|, \quad \bar{A} = c^3A/b^4, \quad \bar{B} = c^3B/b^4, \quad \bar{D} = b^2D/c, \quad \bar{a} = ca/b^2. \quad (3)$$

Henceforth, the redefined parameters and variables are given without overlines. The final expression for the free-energy density takes the form

$$F = A\cos\varphi + B\cos^2\varphi + D\cos\varphi(e_2^2 + e_3^2)/2 + a(e_2^2 + e_3^2)/2 + \operatorname{sgn}be_3(e_3^2 - 3e_2^2)/3 + (e_2^2 + e_3^2)^2/4. \quad (4)$$

The above rearrangement allowed us to eliminate the parameters c and b from the expression for energy. The function $\operatorname{sgn}b$ is necessary for taking into account the sign of the parameter b. In the subsequent discussion, we assume that the generalized fourth-order elastic modulus is $c > 0$.

To find all of the equilibrium states, functional (4) should be minimized with respect to the remaining order parameters $e_{2,3}$ and φ. The minimization resulted in nine equilibrium states, in which the test system can occur, namely:

(1) The ferromagnetic cubic (FC) phase

$$\varphi = 0, \quad e_2 = e_3\,0$$

is stable at $A \le -2B$ and $a \ge -D$.

(2) The ferromagnetic tetragonal (FT) phase

$$\varphi = 0, \quad e_2 = 0,$$

$$e_3 = e_T = (-\operatorname{sgn}b \pm \sqrt{1 - 4(a + D)})/\times 2.$$

(3) The ferromagnetic rhombic (FR) phase

$$\varphi = 0, \quad e_2^2 = 3e_3^2,$$

$$e_3 = e_R = (\operatorname{sgn}b \pm \sqrt{1 - 4(a + D)})/4.$$

The FT and FR phases are stable at $A \le -2B - (D/8)(1 + \sqrt{1 - 4(a + D)})^2$ and $a \le 1/4 - D$.

(4) The antiferromagnetic cubic (AFC) phase

$$\varphi = \pi, \quad e_2 = e_3 = 0$$

is stable at $A \ge 2B$ and $a \ge D$.

(5) The antiferromagnetic tetragonal (AFT) phase

$$\varphi = \pi, \quad e_2 = 0,$$

$$e_3 = e_{AT} = (-\operatorname{sgn}b \pm \sqrt{1 - 4(a - D)})/2.$$

(6) The antiferromagnetic rhombic (AFR) phase

$$\varphi = \pi, \quad e_2^2 = 3e_3^2,$$

$$e_3 = e_{AR} = (\operatorname{sgn}b \pm \sqrt{1 - 4(a - D)})/4.$$

The AFT and AFR phases are stable at $A \ge 2B - (D/8)(1 + \sqrt{1 - 4(a - D)})^2$ and $a \le 1/4 + D$.

(7) The canted antiferromagnetic cubic (CAFC) phase

$$\cos\varphi = -A/2B, \quad e_2 = e_3 = 0$$

is stable at $A \ge -2B$, $A \le 2B$, $B \ge 0$, and $A \le 2Ba/D$.

(8) The canted antiferromagnetic tetragonal (CAFT) phase

$$\cos\varphi = -(A + De_3^2/2)/2B, \quad e_2 = 0,$$

$$e_3 = e_{CT} = (-\operatorname{sgn}b \pm \sqrt{1 - 4\tilde{a}\tilde{c}})/2\tilde{c}.$$

(9) The canted antiferromagnetic rhombic (CAFR) phase

$$\cos\varphi = -(A + D(e_2^2 + e_3^2)/2)/2B, \quad e_2^2 = 3e_3^2,$$

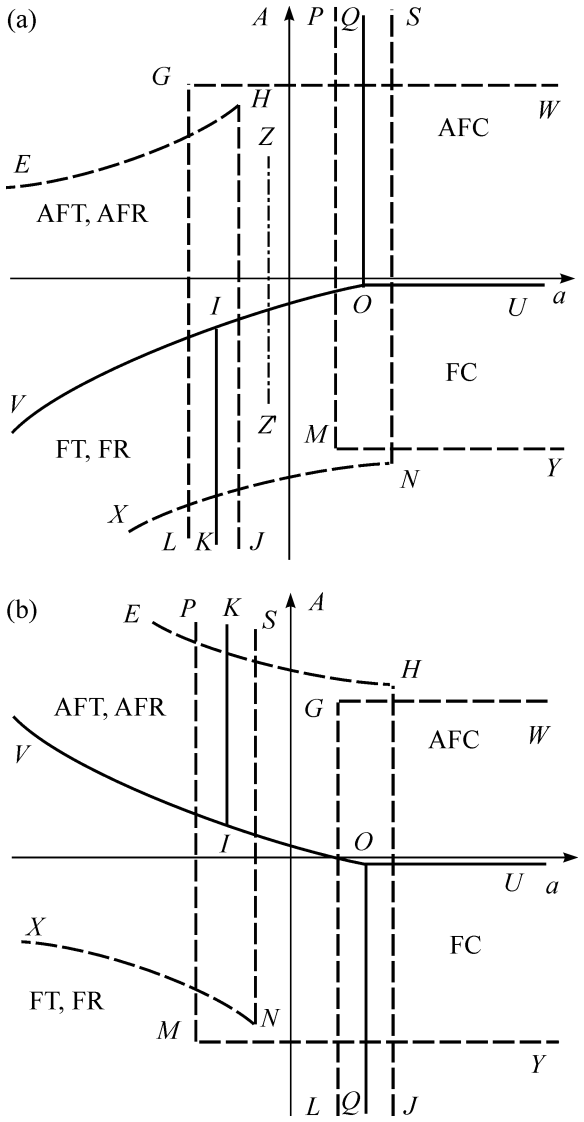

Fig. 1. Schematic phase diagrams for $B < 0$ and (a) $D > 0$ and (b) $D < 0$.

$$e_3 = e_{CR} = (\operatorname{sgn} b \pm \sqrt{1 - 4\tilde{a}\tilde{c}})/4\tilde{c}.$$

The CAFT and CAFR phases are stable at $A \geq -2B - (D/8)(1 + \sqrt{1 - 4(a + D)})^2$, $a \leq 1/4 - D$; $A \leq 2B - (D/8)(1 + \sqrt{1 - 4(a - D)})^2$, $a \leq 1/4 + D$; $A \geq 2Ba/D - B/2\tilde{c}\,D$, $B \geq D^2/4$. Here, $\tilde{a} = a - DA/2B$ and $\tilde{c} = 1 - D^2/4B$.

From an analysis of phase stability regions, it follows that the sign of the parameter b is responsible for only the sign of tetragonal strains e_3 in phases, and it has no effect on the shape of phase diagrams. At $b > 0$, the strains e_3 are positive in the FR, AFR, and CAFR phases and negative in the FT, AFT, and CAFT phases. At $b < 0$, the signs of the strains e_3 in the given phases are reversed. The phase stability regions also suggest that canted antiferromagnetic phases occur only at the positive values of the parameter B. At the negative values of the parameter B in alloys with the inversion of the exchange interaction, six states can occur: three ferromagnetic (FC, FT, and FR) and three antiferromagnetic (AFC, AFT, and AFR) states. The CAFT and CAFR phases occur at $B \geq D^2/4$.

The lines of phase transitions can be determined from a comparison of phase energies. They have the following forms:

$$1\text{–}2(3):\ a = 2/9 - D;$$

$$1\text{–}4:\ A = 0;$$

$$1\text{–}5(6):\ A = (1/24)|e_{AT}|^3(2 - 3|e_{AT}|);$$

$$1\text{–}7:\ A = -2B;$$

$$1\text{–}8(9):\ A = -2B \pm \sqrt{(1/3)B|e_{CT}|^3(2 - 3\tilde{c}|e_{CT}|)},$$

$$A \leq 2Ba/D - 4B/9D\tilde{c};$$

$$2\text{–}4:\ A = (1/24)|e_T|^3(3|e_T| - 2);$$

$$2\text{–}5(6):\ A = (1/24)(|e_{AT}|^3(2 - 3|e_{AT}|) - |e_T|^3(2 - 3e_T));$$

$$2\text{–}7:\ A = \pm\sqrt{(1/3)B|e_T|^3(3|e_T| - 2)} - 2B,$$

$$a \leq 2/9 - D;$$

$$2\text{–}8(9):\ A = \pm((1/3)B[|e_{CT}|^3(2 - 3\tilde{c}|e_{CT}|)$$

$$-|e_T|^3(2 - 3|e_T|)])^{1/2} - 2B,$$

$$|e_{CT}|^3(2 - 3\tilde{c}|e_{CT}|) - |e_T|^3(2 - 3|e_T|) \geq 0;$$

$$4\text{–}5(6):\ a = 2/9 + D;$$

$$4\text{–}7:\ A = 2B;$$

$$4\text{–}8(9):\ A = 2B \pm \sqrt{(1/3)B|e_{CT}|^3(2 - 3\tilde{c}|e_{CT}|)},$$

$$A \leq 2Ba/D - 4B/9D\tilde{c};\quad a \leq 2/9 + D;$$

$$5\text{–}8(9):\ A = \pm((1/3)B[|e_{CT}|^3(2 - 3\tilde{c}|e_{CT}|)$$

$$-|e_{AT}|^3(2 - 3|e_{AT}|)])^{1/2} + 2B,$$

$$7\text{–}8(9):\ A = 2Ba/D - 4B/D\tilde{c}.$$

Figures 1a and 1b schematically represent phase diagrams in the A–a coordinates in the cases of $B < 0$, $D > 0$ and $B < 0$, $D < 0$, respectively. Henceforth, solid lines in phase diagrams are the lines of phase transitions and dashed lines show the boundaries of stability regions. In Fig. 1, it can be seen that the following six equilibrium states can occur in an alloy at $B < 0$: FC, FT (FR), AFC, and AFT (AFR). The FC phase is stable in the region restricted by the lines *LG* and *GW*. The AFC phase is stable in the region on the right of the line *PM* and above the line *MY*. The FT and FR phases are stable

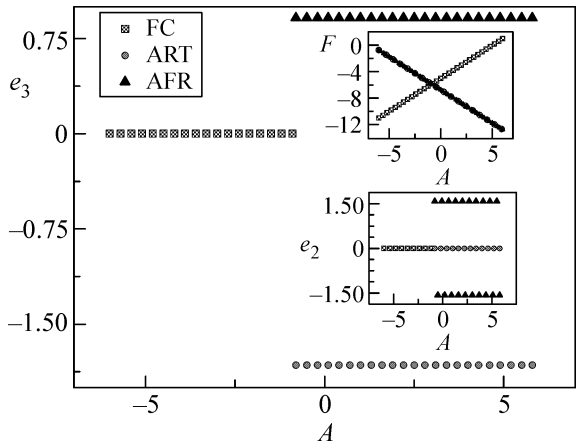

Fig. 2. Strains e_3 and (bottom inset) e_2 and (top inset) the energy density F vs. the parameter A in the thermodynamic path ZZ' (Fig. 1) at $B = -5$ and $D = 1$.

in the region restricted by the lines EH and HJ. The AFT and AFR phases are stable in the region on the left of the line SN and above the line NX. From Fig. 1, it follows that the following phase transitions can occur in the phase diagram: from the FC phase to the AFC phase on the line OU; a phase transition from the FC (Fig. 1a) or AFC phase (Fig. 1b) to the AFT (AFR) (Fig. 1a) or FT (FR) phase (Fig. 1b), respectively, on the line OI; a phase transition from the FC (Fig. 1a) or AFC phase (Fig. 1b) to the FT (FR) (Fig. 1a) or AFT (AFR) phase (Fig. 1b), respectively, on the line IK; and a phase transition from the AFC (Fig. 1a) or FC phase (Fig. 1b) to the AFT (AFR) (Fig. 1a) or FT (FR) phase (Fig. 1b), respectively, on the line OQ. A phase transition between the AFT (AFR) and FT (FR) phases along the line VI also takes place. All of the above transitions are first-order phase transitions.

Let us consider the path ZZ' in Fig. 1a. Figure 2 shows the dependence of the order parameters e_2 and e_3 and the energy F on the parameter A along this path. It can be seen that the FC phase is converted into the AFT or AFR phase by a first-order phase transition on the line IO. The transition is accompanied by an abrupt change in the order parameter e_3 (and e_2 in the transition to the AFR phase) (Fig. 2). Note that this transition was observed experimentally by Kainuma et al. [5] in a Ni–Co–Mn–In alloy. From the results obtained by Kainuma et al. [5], it follows that magnetization in a low-temperature phase was practically equal to zero even in a comparatively strong magnetic field of 70 kOe (see Fig. 1 in [5]) and a pronounced hysteresis was observed in the transition. This suggests that, indeed, a first-order phase transition from the FC phase to the AFT (AFR) phase takes place in the Ni–Co–Mn–In alloy. Kainuma et al. [5] noted that a low-temperature phase in the Ni–Co–Mn–In alloy was modulated and exhibited monoclinic distortions. Here, we ignore the effect of crystal lattice modulation on phase diagrams [1, 4]. However,

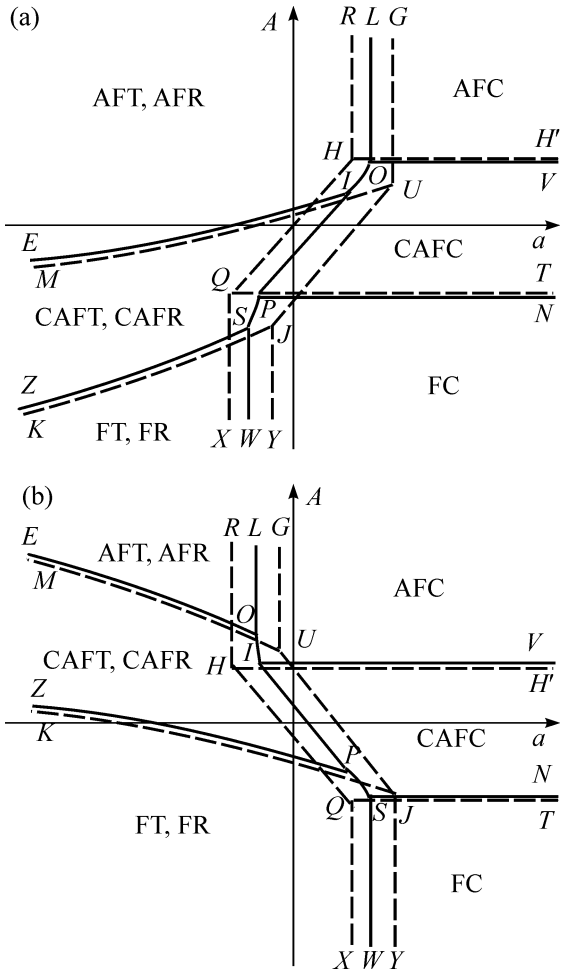

Fig. 3. Schematic phase diagrams for $B > 0$ ($B > 4D^2$) and (a) $D > 0$ and (b) $D < 0$.

monoclinic distortions may be due to anisotropic magnetostriction, which was ignored here. The complete analytic solution of this problem is impossible with consideration for anisotropic magnetostriction. The effects of crystal lattice modulation and anisotropic magnetostriction on phase diagrams will be reported elsewhere.

Figures 3a and 3b show phase diagrams for the cases of $B > 0$, $D > 0$ and $B > 0$, $D < 0$. It can be seen that, indeed, all of the nine equilibrium states can occur in an alloy at $B > 0$.

The FC phase is stable in the region restricted by the lines XQ and QT. The AFC phase is stable in the region on the right of the line HR and above the line HH'. The FT and FR phases are stable in the region restricted by the lines KJ and JY. The AFT and AFR phases are stable in the region on the left of the line GU and above the curve MU. The CAFC phase is stable in the region on the right of the line HQ and between the lines HH' and QT. Finally, the CAFT and CAFR phases occur in the region on the left of the curve JU and between the

curves *MU* and *KJ*. From Fig. 3, it follows that the following phase transitions can occur in a phase diagram at $B > 0$: a second-order phase transition from the FC phase to the CAFC phase on the lines *PN* (Fig. 3a) and *SN* (Fig. 3b); a first-order phase transition between the FC and FT (FR) phases on the line *WS*; a first-order phase transition from the FC phase to the CAFT (CAFR) phase (Fig. 3a) or from the FT (FR) phase to the CAFC phase (Fig. 3b) on the line *SP*; a second-order phase transition between the AFC and CAFC phases along the lines *OV* (Fig. 3a) and *IV* (Fig. 3b); a first-order phase transition from the AFC phase to the AFT and AFR phases along the line *LO*; a first-order phase transition from the CAFC phase to the AFT (AFR) phase (Fig. 3a) or from the AFC phase to the CAFT and CAFR phases (Fig. 3b) along the *OI* line; a first-order phase transition between the CAFC and CAFT (CAFR) phases on the line *IP*; a second-order phase transition from the AFT (AFR) phase to the CAFT (CAFR) phase on the lines *EI* (Fig. 3a) and *EO* (Fig. 3b); and a second-order phase transition between the FT (FR) and CAFT (CAFR) phases on the lines *ZS* (Fig. 3a) and *ZP* (Fig. 3b).

Recall that the CAFT (CAFR) phase occurs only at $B \geq D^2/4$; therefore, phase diagrams do not contain the above phases when the reverse inequality is satisfied. In the latter case, phase diagrams can be constructed in accordance with the lines of the loss of phase stability and the above lines of phase transitions. They are beyond the scope of this communication.

Note that, as follows from Fig. 3a, a transition from the high-temperature FC phase to the CAFT (CAFR) phase can occur in alloys with the inversion of the exchange interaction (Fig. 3a, line *SP*). In this transition, magnetization in the antiferromagnetic phase is lower than that in the ferromagnetic phase but much higher than magnetization in the antiferromagnetic phase in the FC–AFT (AFR) transition shown in Fig. 1a (line *OI*). This is due to the fact that the ferromagnetism vector $\mathbf{M} = \mathbf{M}_1 + \mathbf{M}_2$ is nonzero in the CAFT (CAFR) phase, whereas it is equal to zero in the AFT (AFR) phase. It is likely that the FC–CAFT (CAFR) transition was observed experimentally in Ni–Mn–Sn, Ni–Mn–In, and Ni–Mn–Sb alloys [10–12], in which weak-field magnetization in a low-temperature phase is nonzero but remains much lower than that in a high-temperature ferromagnetic phase in comparatively strong fields.

Thus, in this work, the phase diagrams of the Heusler alloys in which the inversion of the exchange interaction can occur have been theoretically analyzed using the phenomenological Landau theory of phase transitions. It has been shown that the shape of phase diagrams in these alloys depends on the magnitudes and signs of parameters in the Landau functional. At certain magnitudes and signs of the parameters of the Landau functional, the resulting phase diagrams exhibit thermodynamic paths that make it possible to explain the experimentally observed phase transitions in the Ni–Co–Mn–In, Ni–Mn–In, Ni–MN–Sn, and Ni–MN–Sb Heusler alloys [5, 10–12].

This work was supported by the US Civilian Research and Development Foundation (grant no. Y2-P-05-19), the Russian Foundation for Basic Research (project nos. 05-08-50341, 06-02-16266, 07-02-96029-r-ural, and 06-02-39030-GFEN), the Council of the President of the Russian Federation for Support of Young Scientists and Leading Scientific Schools (project no. MK-5658.2006.2), and the Human Capital Foundation.

REFERENCES

1. P. Entel, V. D. Buchelnikov, V. V. Khovailo, et al., J. Phys. D: Appl. Phys. **39**, 865 (2006).
2. V. D. Buchel'nikov, A. N. Vasil'eva, V. V. Koledov, et al., Usp. Fiz. Nauk **176**, 900 (2006) [Phys. Usp. **49**, 871 (2006)].
3. A. N. Vasil'ev, A. D. Bozhko, V. V. Khovailo, et al., Phys. Rev. B **59**, 1113 (1999).
4. A. N. Vasil'ev, V. D. Buchel'nikov, T. Takagi, et al., Usp. Fiz. Nauk **173**, 577 (2003) [Phys. Usp. **46**, 559 (2003)].
5. R. Kainuma, Y. Imano, W. Ito, et al., Nature **439**, 957 (2006).
6. V. V. Khovaylo, V. D. Buchelnikov, R. Kainuma, et al., Phys. Rev. B **72**, 224408 (2005).
7. C. Kittel, Phys. Rev. **120**, 335 (1960).
8. H. S. Jarrett, Phys. Rev. [Sect. A] **134**, A942 (1964).
9. W. A. Doerner and R. B. Flippen, Phys. Rev. [Sect. A] **137**, A926 (1965).
10. Y. Sutou, Y. Imano, N. Koeda, et al., Appl. Phys. Lett. **85**, 4358 (2004).
11. T. Krenke, M. Acet, E. F. Wassermann, et al., Phys. Rev. B **72**, 014412 (2005).
12. P. J. Brown, A. P. Gandy, K. Ishida, et al., J. Phys.: Condens. Matter **18**, 2249 (2006).

Translated by V. Makhlyarchuk

SPELL: OK